MATERIALS FORUM VOLUME 33 - 2009
Edited by Dr Steve Galea, Associate Professor Wingkong and Professor Akira Mita

DESIGN OF THE ACOUSTIC ELECTRIC FEEDTHROUGH DEMONSTRATOR MK II

Scott Moss, Chris Phoumsavanh, Michael Konak, Kelly Tsoi, Nik Rajic, Steve Galea, Ian Powlesland, Phillip McMahon[1]

Air Vehicles Division, [1]Maritime Platforms Division,
Defence Science and Technology Organization,
506 Lorimer St, Fishermans Bend, Victoria, 3207

ABSTRACT

This report outlines the preliminary design of the DSTO Acoustic Electric Feedthrough (AEF) Laboratory Demonstrator Mk II which will pass power, and transfer data, through metal plate using ultrasound. It is envisaged that the AEF approach will allow wireless powering and communications with in situ structural health monitoring systems embedded within aircraft and other high value assets. This paper discusses the modelling and characterization measurements which fed into the design of the Mk II demonstrator, as well as the design itself.

1 BACKGROUND

The Australian Defence Science and Technology Organization (DSTO) is developing in situ structural health monitoring (SHM) systems[1-5] for potential use in high value platforms across the Australian Defence Force. A recent output from this DSTO program is the Compact Multi Parameter Load Evaluation unit (CMPLE)[6], which is an autonomous flight loads and acceleration measurement module that was flight trialed on a Royal Australian Air Force (RAAF) DHC-4 Caribou aircraft in mid-2008. The flight trial plan involved: (i) the rapid installation of CMPLE units at various external locations on an aircraft, (ii) the downloading of data after each test flight for post processing of the flight load and acceleration data, and (iii) the easy removal of the units at the end of the flight trial. The flight data from this low cost technology is being used to assist the structural integrity management of the Caribou fleet which is necessary to enable Australia to continue operating this aging, yet highly versatile, tactical transport aircraft. It is imagined that a future enhanced version of the CMPLE system could be employed to: (i) continuously monitor airframe loads and accelerations during flight, (ii) detect damage and damage growth and other structural problems, and (iii) provide a basis for near-real-time damage assessment. This technology could also potentially permit a safe reduction in inspection and regular maintenance costs and therefore substantially impact on aircraft through-life support costs.

To increase the usefulness of the CMPLE system, an Acoustic Electric Feedthrough (AEF)[7,8] system is being investigated as a means of providing power and two way communications to a CMPLE unit that has been mounted at a location where physical access is difficult. For example, an AEF system could provide power and communications through the skin of an aircraft to a CMPLE unit mounted on structure located inside the aircraft. The AEF arrangement was initially proposed by Hu *et al*[9] who modelled an AEF from first principles; the model was later advanced by Sherrit *et al*.[10] The AEF model implemented by Hu *et al* and Sherrit *et al* consisted of a metal plate sandwiched between two piezoelectric layers. Sherrit *et al* highlighted the fact that their modelling did not incorporate adhesive bondlines between the piezoelectric material and the metal plate. DSTO examined the effect of adhesive bondlines by modelling the AEF arrangement using LTSpice[11], and found that the bondlines significantly affect the behaviour of an AEF arrangement.[7] Further explorations were also carried out using the LTSpice AEF models with the aim of optimizing the power transmission efficiency through thin metal plates.

Moss *et al*[8] discusses the manufacture of the *AEF Demonstrator Mk I*, which was designed to showcase acoustic power transfer through a metal plate. Using the previous DSTO AEF investigations as a basis, this paper will discuss the design of the *AEF Laboratory Demonstrator Mk II* that will use ultrasound to transmit power and two-way communications across a metal plate.

1.1 LTSpice Modelling of an Acoustic Electric Feedthrough (AEF)

As mentioned, the use of LTSpice produced AEF models with superior predictive capability compared to those presented in the literature because of: (i) the addition of extra AEF layers (i.e. bondlines), (ii) the addition of realistic electrical components in the model and (iii) the use of lossy-transmission-lines to model damping.[11,13]
Figure 1 is a schematic cross-section of the *physical interface* of an AEF system showing the transmit and receive Lead Zirconate Titanate (PZT) elements bonded either side of a metal plate. For clarity, the AEF demonstrator will be considered to have three main sub-components: (i) a *transmitter*, (ii) a *physical interface* and (iii) a *receiver*. Figure 2 shows a schematic example

of the AEF model that was implemented in LTSpice showing the three main sub-components encircled by dashed lines. The *transmitter* is the electronics that is used to drive the transmit PZT element. The *physical interface* is the acoustic path along which the ultrasound travels, with a distance equal to the combined thicknesses of: (i) the transmit and receive PZT elements, (ii) the aluminium plate, and (iii) the adhesive bondlines. The *receiver* is the electrical circuitry that is attached to the receive PZT element.

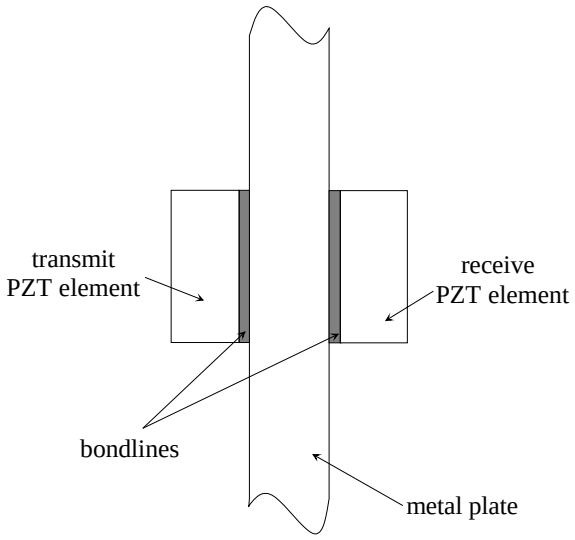

Figure 1. Schematic showing the Physical Interface of an Acoustic Electric Feedthrough (AEF).

The LTSpice model shown in Figure 2 includes a constant apparent power *transmitter*, a non-linear electrical load for the *receiver*, and realistic bondline thicknesses (labelled as *LossyBondTline*). This level of model fidelity was required to achieve reasonable correlation with the measured AEF power transfer results. Further information on the LTSpice modelling on AEF systems can be found in Moss *et al* [7]. Pz27 was the initially chosen to form the AEF demonstrator due to it being a general purpose PZT material.[14] Manufacturer specified piezoelectric parameter values were used for modelling and can be found in the Appendix. To simulate a frequency sweep with the LTSpice model, a script was written that would step the *transmitter* drive frequency over the range 600 kHz -1300 kHz with 5 kHz increments.

A number of factors were found to have significant influence on the efficacy of the AEF modelling. These factors are summarized here and discussed in more detail in Moss *et al*[7]:

(i) A*dhesive bondline* - nominal bondline thicknesses of 100 µm were used in the LTSpice model shown in Figure 2. The bondlines were assumed to be silver loaded epoxy[15], with material properties given by Rajic[16] (see Appendix).

(ii) *Supply impedance* – the power amplifier used for experimental characterization of the AEF *physical interface* had an output impedance of 50 Ω.

(iii) *Constant power source* – to supply a constant apparent input power.

(iii) *Material damping* – damping in the PZT elements, aluminium plate and adhesive bondlines are modelled using lossy-transmission-lines.

(v) *Diodes* – high speed 1N5818 Schottky diodes[17] were used to create the rectifying bridge on the receive side of the plate to maximize the AEF power transfer efficiency.

(vi) *Load resistance* – a high frequency 1 µF capacitor was used to store electrical charge. Characterization measurements utilized an optimized resistive load R1 to maximize power transfer.

(vii) *PZT element geometry* – a constant PZT element geometry consisting of a disk of diameter 38 mm and a thickness of 2 mm was used during all investigations described in this paper. The 2 mm PZT element thickness was chosen because it has a fundamental anti-resonant frequency of approximately 1 MHz, low enough to ensure that cable-inductance issues were negligible and that the transmitter circuitry used in the AEF demonstrator could be simplified through the use of commercially available MOSFET driver chips.

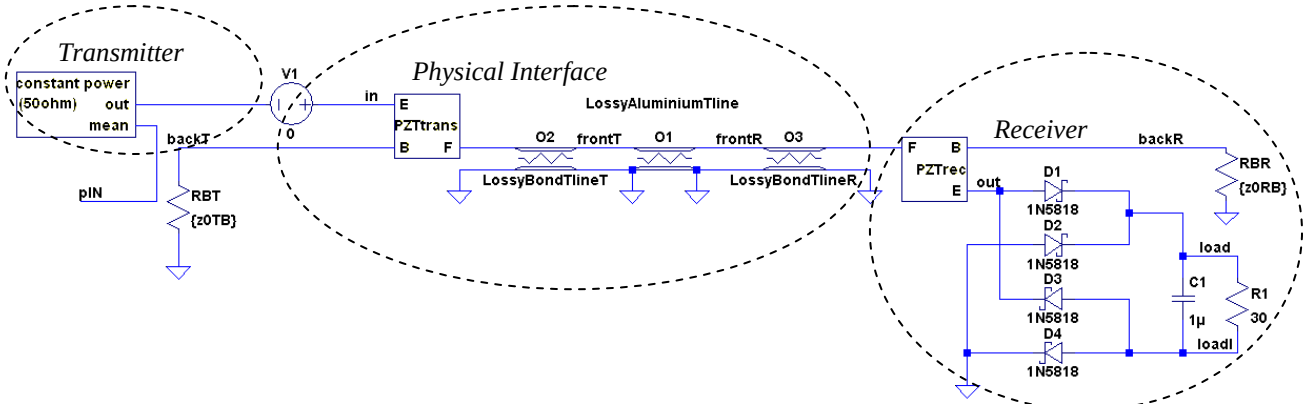

Figure 2. LTSpice schematic of a PZT/Aluminium/PZT AEF system with a constant 1 W apparent input power and diode bridge RC load. The three main sub-components of an AEF arrangement are encircled: the transmitter, the physical interface and the receiver.

2 EXPERIMENT

This section examines the laboratory measurements required to characterize the AEF system, the results of which fed into design of the hardware being developed for the AEF demonstrator. The majority of the characterization work was performed on AEF arrangements formed using a 1.6 mm thick aluminium plate, which is representative of the outer skin thickness of a Caribou aircraft. As mentioned earlier, the manufacture of *AEF Demonstrator Mk I* [8] was created to showcase acoustic power transfer through a metal plate. The Mk I demonstrator is depicted in

Figure 3 which shows the three main sub-components. The Mk II demonstrator design includes the same main sub-components, each of which is described below. Also discussed in this section are the measurements undertaken to characterize the thermal behaviour of an AEF arrangement during operation. Finally, there is a discussion of the communications technqiue that will be utilized in the *AEF Demonstrator Mk II*.

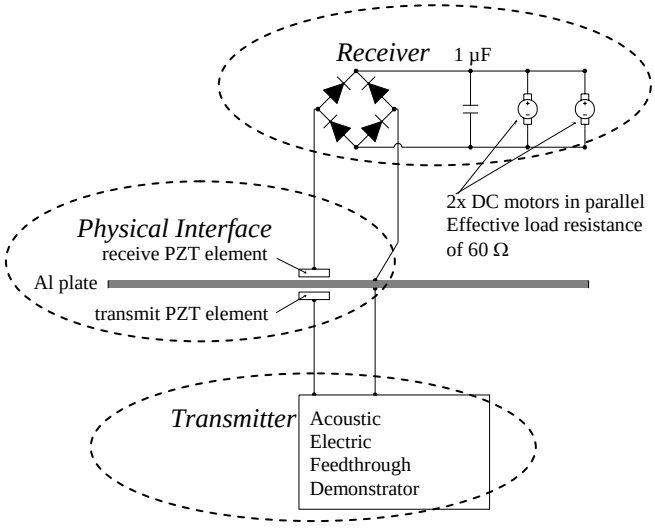

Figure 3. Schematic of AEF Demonstrator Mk I.

2.1 Characterization of the Physical Interface and Receiver

Measurements to characterize the *physical interface* and *receiver* were carried out using an AG1021 100 W power amplifier to drive the transmit PZT element, and are discussed in detail in Moss *et al*[7]. These measurements were necessary to experimentally determine the optimum operating frequency for the AEF demonstrator and to give some indication of the power transfer efficiency that should be expected.

2.2 Power Transmitter Circuit for the Demonstrator

The AEF demonstrator *transmitter* is a battery based circuit that uses a MOSFET- driver chip to electrically excite the transmit PZT element (shown in

Figure 3) at it's through-thickness anti-resonant frequency. For power transfer the *transmitter* is designed to provide approximately 1 W of continuous apparent input power to the PZT element. For communications the *transmitter* is required to generate 260 ns, 10 V pulses. Figure 4 is a schematic of the transmitter circuitry which shows the three main Integrated Chips (IC's) labelled as U1, U2 and U3. The *transmitters*' operation, and a description of the main IC's, is given below:

U1 - the MC34151 is a high speed MOSFET gate driver IC (hereafter called the 'MOSFET driver'), manufactured by Motorola (ON Semiconductor).[18] This IC has a 1.5 A totem pole output stage and can drive a 1 nF capacitive load with rise and fall times of 15 ns. Input drive signal levels are CMOS/LSTTL compatible.

U2 - the LTC6902 is a precision, low-power, stable oscillator IC, manufactured by Linear Technology.[19] The oscillator frequency is adjusted by the use of a trim-pot variable resistance (resistor R3 in Figure 4). The oscillator frequency can be varied from 900 kHz to 1200 kHz.

U3 – the LP2950 is a micro-power, low-dropout voltage, 5 V voltage regulator used to provide a regulated 5 V supply for the oscillator IC, and is manufactured by National.[20]

A matching circuit consisting of a series inductor and parallel load capacitor is used to match the effective input impedance of the transmit PZT element to the MOSFET driver. The matching network component values are selected to yield a transfer function (between input and output) that has a peak resonance occurring at the operating frequency used to transfer power. The matching circuit also converts the square wave drive signal from the MOSFET driver to a sinusoidal waveform across the transmit PZT element.

Figure 5 is a photograph of the completed power transmitter circuit layout and shows the two rechargeable nickel-metal-hydride batteries used to power the circuit. The completed *transmitter* sub-component is shown in
Figure 6 wired to the transmit PZT element. When the *transmitter power-on button* is pushed an LED lights up indicating that the transmitter circuit is energized and

that a sinusoidal voltage with an approximate frequency of 1000 kHz is being applied to the transmit PZT element. The transmit PZT element electromechanically converts the applied sinusoidal voltage to ultrasound, which is then acoustically transmitted across the AEF *physical interface*.

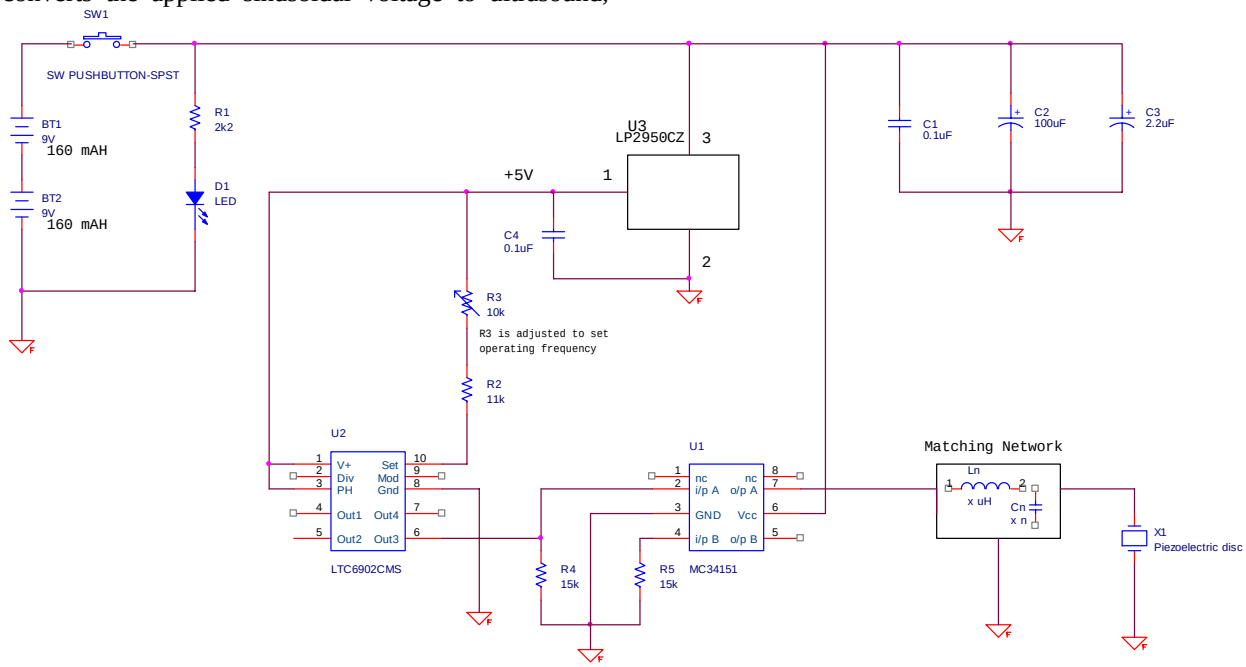

Figure 4. Transmitter circuitry for the AEF demonstrator.

2.3 Physical Interface of Demonstrator

Details of the manufacture of the AEF *physical interface* are given in Moss *et al*[7]. In summary: two *well matched* Pz27 disks with 38 mm diameter and 2 mm thickness were chosen, where *well matched* refers to the matching of the fundamental thickness-mode resonance and anti-resonance peaks of the two Pz27 disks. Silver-cermet was chosen as the electrode material for the Pz27 disks because it is easily soldered. The disks were bonded to either side of the metal plates using silver loaded epoxy[15], with the disk centres axially collocated to within 1 mm. Square aluminium plate was used, with thickness 1.6 mm and side length 600 mm. After ultrasound passes through the *physical interface* it arrives at the receive PZT element where it is electromechanically converted from a stress wave into a voltage across the *receiver* circuit.

2.4 Power Receiver Circuit for the Demonstrator

As described earlier, and shown schematically in

Figure 3, the *receiver* circuit is a fully rectifying diode bridge with a high frequency 1 µF storage capacitor and a resistive load. The electrical load for the Mk I demonstrator was supplied by two small electric motors with an equivalent total resistance of 60 Ω. The electrical load for the Mk II demonstrator will be a small Lithium-ion battery, which will used to power the CMPLE device.

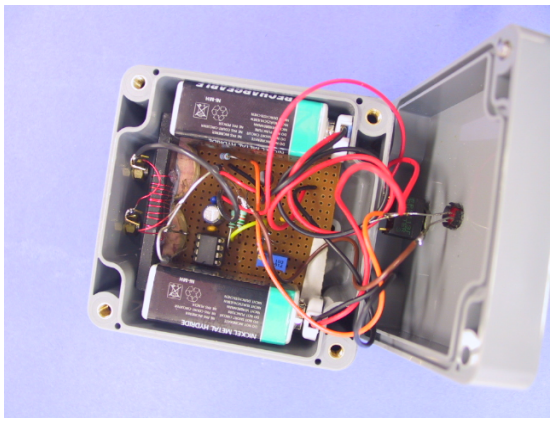

Figure 5. Internal layout and wiring of the transmitter circuit for the AEF demonstrator.

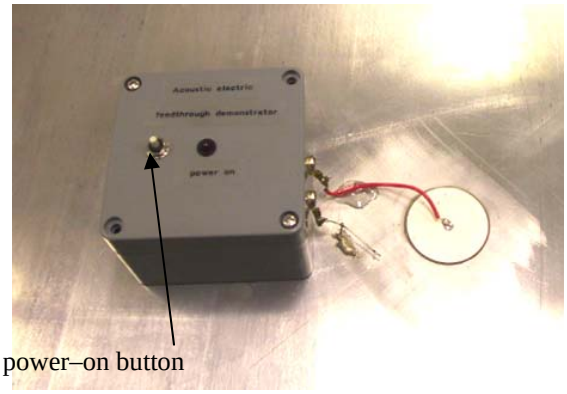

Figure 6. Picture of the assembled AEF demonstrator's transmitter showing the connection to the physical interface.

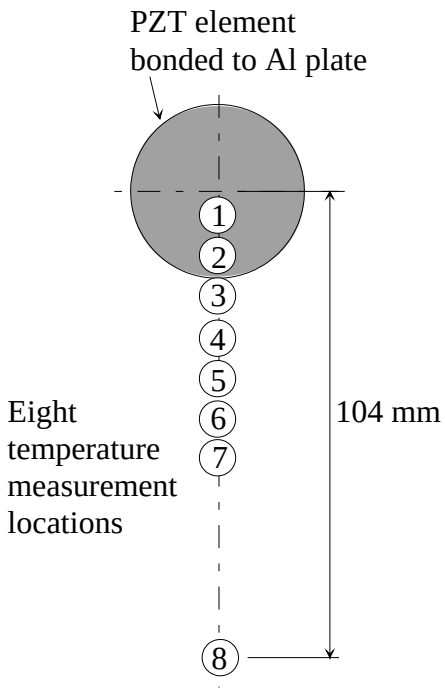

(a) (b)

Figure 7. (a) Photograph of the experimental arrangement used for thermal measurement of a Pz27 based AEF system and the surrounding metal plate and (b) schematic showing the 38 mm diameter receive Pz27 element and the location of temperature measurement spots.

2.5 Thermal Measurements of the Physical Interface

A series of measurements were made to understand the level of temperature increase that may be experienced by an operating AEF arrangement and its surrounding region.

Figure 7a shows a photograph of the experimental arrangement; an uncooled micro-bolometer infra-red (IR) detector was set up to measure temperature as a function of time on the *receiver* side of the plate, which was painted with a matt-black paint (with a nominal emissivity of 0.92[21]) to reduce the effect of emissivity variations. Aluminium plate thickness for these measurements was 1.6 mm. The experiment was carefully arranged to minimize thermal reflections and airflow across the plate. The *transmitter* power for the thermal measurements was increased from 1 W to 3 W, and was expected to generate a proportionally larger temperature rise. Figure 7b shows the position of the spot temperature measurements relative to the receive PZT element, with measurement spots 1 and 2 located on the PZT element and spots 3-8 located on the aluminium plate. The spot diameter was 8 mm.

2.6 Communications

A simple communications technique was proposed and then simulated in LTSpice using a model similar to that shown in Figure 2. Experimental validation of the communications model was carried out and then a circuit board was designed to verify the operational effectiveness of the proposed communications technique. AEF communications will be further discussed in detail in section 3.

3 RESULTS AND DISCUSSION

This section is divided into three main parts. The first part compares the measured and modelled power transfer through an AEF arrangement that uses 2 mm thick Pz27 disks. The second part examines both the measured and modelled power loss mechanisms that reduce the power transfer efficiency of an AEF system which leads to the adoption of a different PZT material. The third part investigates communication strategies that will be implemented in the *AEF Demonstrator Mk II*.

3.1 Measured and Simulated Power Transmission

Simulations were carried out using the LTSpice AEF model shown in Figure 2 and comparison was made with laboratory data measured using the experimental setup shown in Figure 8a. The results presented in this section pertain to an AEF arrangement formed using Pz27 disk elements that had 38 mm diameter and 2mm thickness and 1.6 mm thick aluminium plate. Later in this paper there will be a discussion of an AEF arrangement formed using a harder piezoelectric material, Pz26[14] (see the Appendix for piezoelectric material parameters).

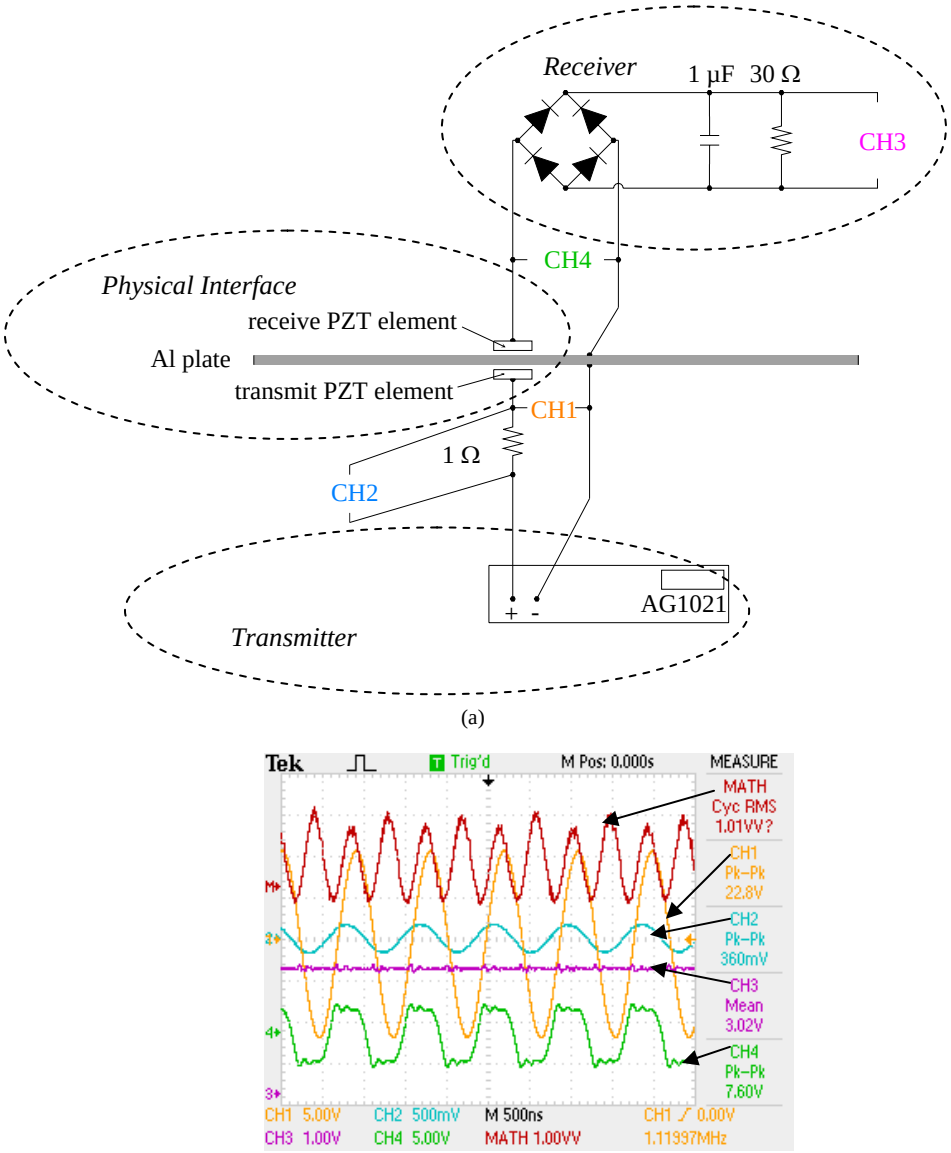

Figure 8. (a) Schematic of the experimental setup used to characterize both the physical interface and the receiver of the AEF demonstrator and (b) oscilloscope screen capture showing example voltage traces from a characterization experiment that was performed using a Pz27 based AEF with 1 W of input power and a 30 Ω load resistance. Channel locations are indicated in Figure 8a: CH1=V(in), CH2=I(in), CH3=V(out) across 30 Ω, CH4=voltage across the receive PZT element, MATH=V(in)*I(in).

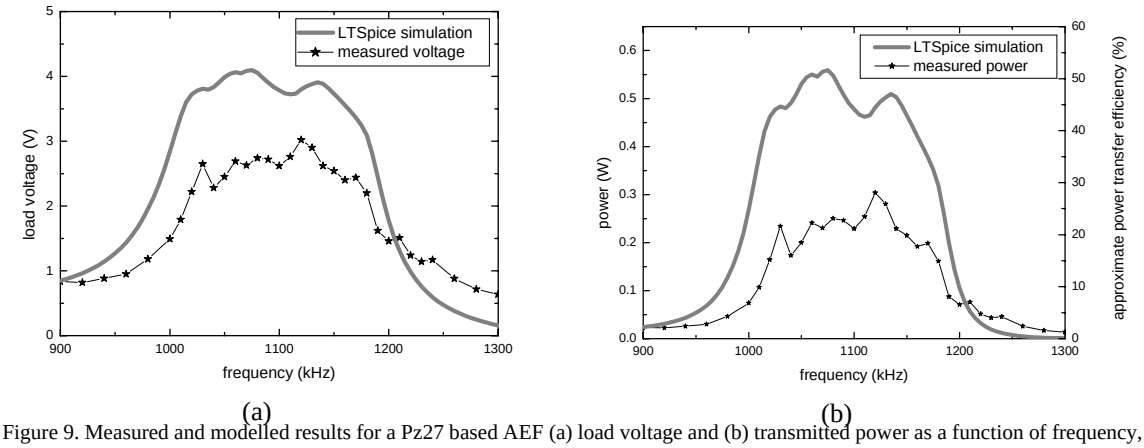

Figure 9. Measured and modelled results for a Pz27 based AEF (a) load voltage and (b) transmitted power as a function of frequency, using a 30 Ω load resistor.

An example of a measured oscilloscope trace is shown in Figure 8b; traces were captured after each increment in drive frequency. Modelled and measured AEF results pertaining to a 1.6 mm thick aluminium plate are shown in Figure 9. The measured data shown in Figure 9 was calculated from a series of traces similar to that shown

in Figure 8b. Figure 9 is a plot of the load voltage as a function of frequency, showing a modelled peak voltage of 4.0 V and a measured peak voltage of 3.0 V.

Plotted in Figure 9b is load power as a function of frequency; because the load voltage had a negligible amount of ripple the power was estimated using the simple relationship $P_{LOAD} = \left(V_{MEAN}^{LOAD}\right)^2 / 30\,\Omega$. The modelled peak power transfer was near 550 mW whereas the measured peak power transfer was just over 300 mW. It is assumed that the difference is the power lost to the metal plate which is not included in the model. The approximate power transfer efficiency $\nu = 100 \times \left(P_{LOAD} / 1W\right)$, shown as a percentage in Figure 9b, is only accurate at the resonant peak where the input current and voltage are in phase and the real input power was 1 W. For the measurement conditions indicated in Figure 8 (i.e. 1 W input power, drive frequency 1120 kHz and 30 Ω load resistance), the measured efficiency was:

$$\nu = 100 \times \left[\left(3.02\,V\right)^2 / 30\,\Omega\right] / 1W = 30.4\,\%.$$

Figure 9b also shows that the measured power transfer peak was centred at 1100 kHz with a Full-Width-Half-Maximum (FWHM) of ~166 kHz, whilst the simulated power transfer peak was centred at 1091 kHz with FWHM ~183 kHz. The layered structure of the AEF *physical interface* is postulated as the cause of the relatively large FWHM. Both the modelled and measured power curves show that the centre of the power transfer peak was located near the anti-resonant frequency of a bonded 2 mm thick Pz27 disk (see Moss *et al*[7] for more details).

An analysis of the various loss mechanisms of the AEF system was carried out to explore the possibility of increasing the power transfer efficiency of the feedthrough and will be discussed next.

3.2 Mechanisms of Power Transmission Loss

3.2.1 Measured Power Transmission Efficiency of the AEF Demonstrator

The measured results presented in this sub-section pertain to the AEF demonstrator itself. Figure 10 plots the measured quiescent current consumption of the AEF demonstrator, as a function of supply voltage, with no electrical load connected, operating at a frequency of 1050 kHz, and with the LED current excluded. From the measured quiescent current consumption the quiescent supply power was calculated to give a maximum of 203 mW at a supply voltage (V_{CC}) of 16 V. To optimize the power transmission efficiency of the AEF demonstrator a *matching network* was used (see Figure 4). Component values for the *matching network* were chosen based on the operating frequency and the input impedance that was measured on the transmit side of the AEF *physical interface* (with the *receiver* circuitry attached to the receive side of the plate with a load resistance of 30 Ω). The input impedance was measured using an input drive signal with a peak of 12 V, which was the approximate level of the drive signal amplitude at the output of the impedance matching network and found to be resistive only at 1050 kHz with a value of 255 Ω. With a load resistance of 255 Ω modelling of the *matching network* (Figure 4) predicted that an inductance of 7.0 µH and capacitance of 3.2 nF were required for optimum transfer efficiency near 1050 kHz. In practice a *matching network* with an inductance of 7 µH and capacitance of 220 pF was found to be effective. A beneficial effect of the *matching network* was that it also had a filtering effect on the output of the transmitter circuit, producing an output that had a more sinusoidal form.

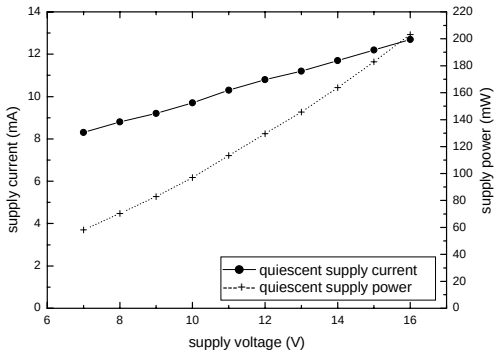

Figure 10. Measured quiescent supply current and quiescent supply power of the AEF demonstrator's transmitter unit, as a function of supply voltage.

With the *matching network* sufficiently optimized the power transfer efficiency of the AEF demonstrator was measured. The three main sub-components of the AEF demonstrator (see Figure 3) were assembled. The maximum supply voltage of the high speed MOSFET driver IC (U1 in Figure 4) is 20 V; to be conservative a supply voltage V_{CC} = 15 V was used, which produced a source current I_{SS} = 43 mA (Figure 4), for a total input power of 645 mW. This input power generated 2.0 V across the 30 Ω load, for a load power of 133 mW. The quiescent power for the *transmitter* with V_{CC} = 15 V was 183 mW. The measured power transmission efficiency for the AEF demonstrator is then,

$$\nu = 100 \times \left[133\,mW / \left(645\,mW - 183\,mW\right)\right] = 28.8\,\%.$$

This value is slightly lower than the power transfer efficiency stated in section 3.1 since the 2.0 V generated across the load means that relatively more power is being consumed in the rectifying diodes. Note also that dynamic power loss in the MOSFET driver is not included in this calculation.

3.2.2 Modelling of Power Losses

The modelling and experimental work presented in this section pertains to an AEF formed with an aluminium

plate of thickness 1.6 mm. Figure 11 shows the modelled variation of load voltage and power as a function of load resistance and transmission frequency. The LTSpice model shown in Figure 2 formed the basis of the modelling, with resistor R1 stepped across the range 1 Ω to 100 Ω, and the transmission frequencies stepped from 1025 kHz to 1150 kHz which corresponds to the frequency range of the main power-transfer peak shown in Figure 9. Figure 11a shows that a 30 Ω load resistor produced modelled load voltages in the range 3.7 V to 4.1 V, which was deemed to be a useful voltage range by the authors as it is matched to lithium polymer battery charging requirements.

Load power as a function of resistance is plotted in Figure 11b where it appears that the load resistance for optimum power transfer efficiency lies somewhere in the range of 30 Ω to 60 Ω and is dependent on the drive frequency. The effective load for the AEF demonstrator was 60 Ω (shown in

Figure 3), which lies at the high end of the load resistance region for optimum efficiency.

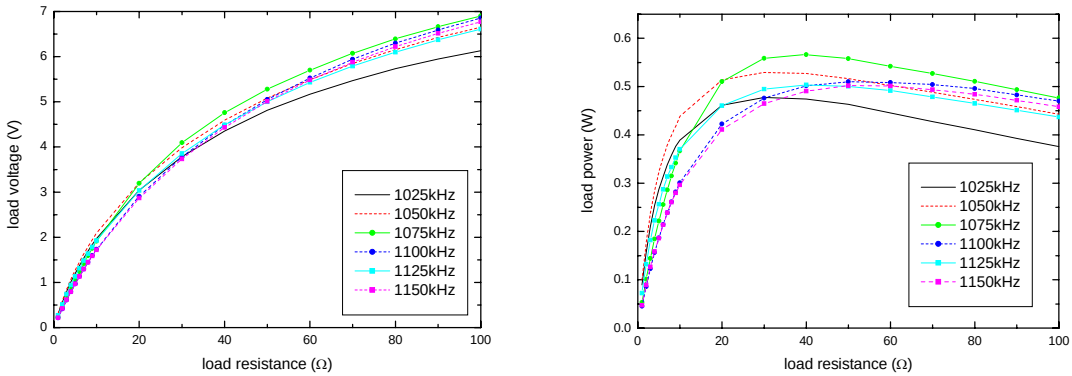

(a) (b)

Figure 11: Modelled results for a Pz27 based AEF, (a) load voltage and (b) load power, with varying load resistance and drive frequency swept across the fundamental thickness resonance, 1025-1150 kHz.

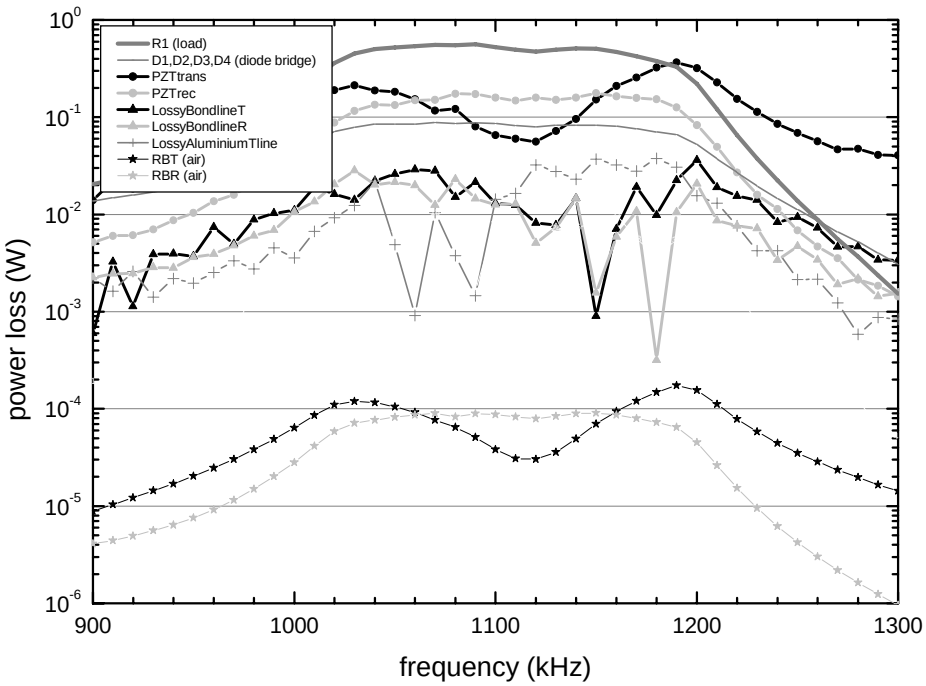

Figure 12. Simulation results showing power loss as a function of frequency for a Pz27 based AEF with 1 W of apparent input power and a 30 Ω load (component labels as per Figure 2).

Figure 12 shows the modelled power loss as a function of frequency for the various components of the LTSpice model shown in Figure 2. Again, the simulations were performed for an AEF arrangement formed using 1.6 mm thick aluminium plate. Although the authors do not consider it a loss, the power consumed in the load

resistor is included in Figure 12 for comparison with the other loss terms. Interestingly, the loss due to mechanical Q of the Pz27 elements appears to be substantial (see PZTtrans and PZTrec in Figure 12); the combined loss of both elements is greater than 200 mW in the frequency range 1020 kHz to 1180 kHz. Over the same frequency range the total diode loss is approximately 80 mW, and other individual component losses are calculated to be approximately 30 mW or less.

Numerical noise in the LTSpice modelling was at the nano-Watt level; note however that some of the components shown in Figure 12 appear to exhibit quite erratic behaviour, in particular the power loss in the aluminium plate and the two bondlines, which requires some explanation. The fluctuation seen in the power loss of these components is an artefact of the calculation used to find the average loss during the simulation. At each frequency step an LTSpice transient analysis was performed over 300 µs and the average value of the power loss in each component was calculated over the last 29 µs. Being electro-mechanical in nature, the LTSpice model (Figure 2) has a variety of different system time constants, each of which has a varying duration. It is hypothesised by the authors that the fluctuation seen in some of the components in Figure 12 is an indication that there was transient behaviour that had not fully stabilized at the end of the first 300 µs, or that there was a beating effect due to reflections of acoustic energy backwards and forwards across the *physical interface*. It should also be noted that the equations used to calculate the power loss in each component do not consider phase difference between through and across variables (i.e. *force and velocity* or *current and voltage*) so variation in phase difference between these variables during the measurement period will also appear as fluctuation in Figure 12.

A significant loss mechanism that has not been explored in this paper is the power loss into the plate that the AEF system is formed on. The reason for this omission is the one-dimensional nature of the LTSpice models used. The difference between the measured and modelled results is assumed to be loss into the plate.

3.2.3 AEF Thermal Measurements

It has been shown that the power transfer efficiency of an AEF arrangement based on 38 mm diameter, 2 mm thick Pz27 disk elements is near 30%. Modelling has indicated that a significant amount of power is lost due to viscous-type material damping within the piezoelectric elements (see Figure 12). It was expected that the viscous power loss within the Pz27 elements might produce a temperature rise in the elements themselves and also in the surrounding metal plate. To test this hypothesis an IR camera was used to measure the temperature of the PZT and plate as a function of time while an AEF arrangement was transmitting power. To perform the measurement 3 W of input power was applied to the AEF arrangement shown in Figure 8a, formed using 1.6 mm thick aluminium plate. The input power was increased to 3 W (compared to the 1 W maximum input power used in other experiments) to generate temperature increases in the PZT and plate that were substantially above the experimental noise, which was approximately 0.1 K.

Figure 13 shows temperature measurements taken at the locations indicated in Figure 7b for a Pz27 based AEF. Temperature was recorded as a function of time and distance from the centre of the receive PZT element. Approximately two minutes after thermal data recording commenced, the ambient PZT and plate temperatures were recorded. Within a few seconds of the ambient temperature measurements being taken, power was applied to the AEF arrangement. Temperature measurements were then recorded at 15 minute intervals. The temperature data in
Figure 13 was logged over approximately 1.5 hours and shows that during this time the temperature near the centre of the Pz27 receive element increased by 4.6 K (measurement location 1), while the far-field plate temperature increase was 2.6 K (measurement location 8). Previous studies have shown: (i) that ambient temperature variations can produce a shift in the resonant frequency of a bonded PZT element[22], and (ii) that temperature variations of approximately 4 K can influence the efficiency of ultrasonic power transfer through a structure.[23]

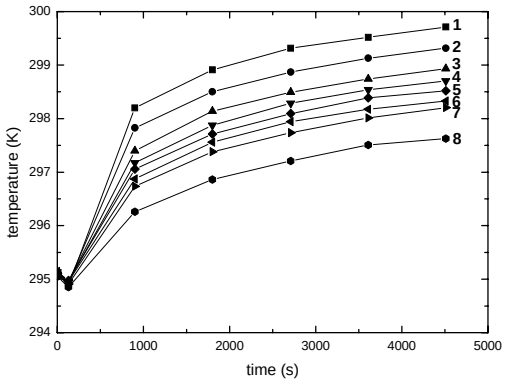

Figure 13. Temperature recorded at the eight measurement locations (corresponding to Figure 7b) as a function of time, for the Pz27 based AEF driven with 3 W of input power.

Oscilloscope traces were recorded after the AEF had been operating for more than 80 minutes under an input power of 3 W. From the measured mean load voltage the efficiency of the AEF arrangement with 3 W of input power was found to be:

$$\nu = 100 \times \left[(5.12\,V)^2 / 30\,\Omega \right] / 3\,W = 29.1\,\%\,.$$

For comparison the efficiency using 1 W of input power was 30.4% (section 3.1). It is postulated that the temperature rise generated by the 3 W of input power might have caused a small change in the anti-resonant frequency of the PZT elements, leading to a de-tuning AEF arrangement, which resulted in a small reduction in power transmission efficiency. Unfortunately direct

comparison between the efficiencies calculated for 1 W and 3 W input power is not possible due to the non-linearity in the *receiver* caused by the rectifying bridge.

3.2.4 Power transfer comparison: Pz27 versus Pz26

Further simulation and measurement was performed to compare the power transfer performance of Pz27 versus other piezoelectric materials. Of particular interest was the hard piezoelectric material Pz26.[14] Pz26 has a mechanical Q~3000 and it was thought that lower material damping might reduce AEF power losses and hence improve the power transfer efficiency. Modelling indicated an optimum load of 75 Ω for an AEF arrangement formed using a Pz26 disk and 1.6 mm aluminium plate. Modelled and measured AEF results for a Pz26 based AEF arrangement are shown in Figure 14a which plots the load voltage as a function of frequency showing a modelled peak voltage of 7.7 V and a measured peak voltage of 5.5 V. Plotted in Figure 14b is the load power as a function of frequency; load power was estimated using:

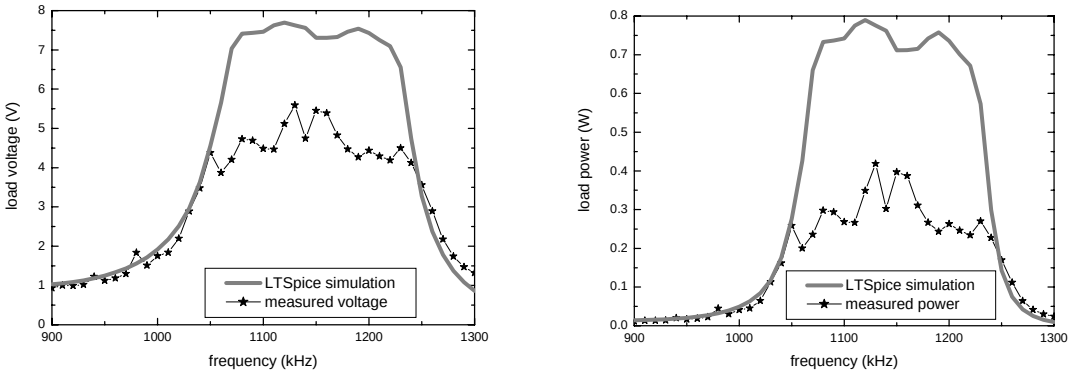

(a) (b)

Figure 14. Measured and modelled results for a Pz26 based AEF (a) load voltage and (b) transmitted power as a function of frequency, using a 75 Ω load resistor.

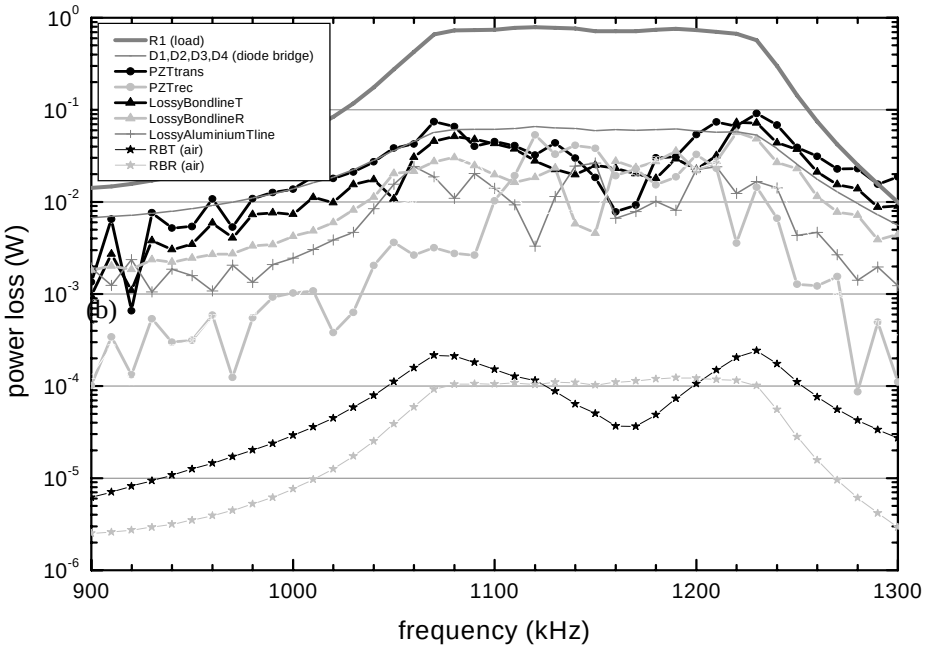

(b)

Figure 15. Simulation results showing power loss as a function of frequency for a Pz26 based AEF with 1 W of apparent input power and a 75 Ω load (component labels as per Figure 2).

$P_{LOAD} = \left(V_{MEAN}^{LOAD}\right)^2 / 75\,\Omega$. The modelled peak power transfer was near 790 mW whilst the measured peak power transfer was just over 400 mW. The measured power transmission efficiency was:

$$\nu = 100 \times \left[(5.46\,V)^2 / 75\,\Omega\right] / 1\,W = 39.7\,\%,$$

which is an improvement on the 30.4 % efficiency calculated for a Pz27 based AEF arrangement (section

3.1).

Figure 15 shows the modelled power losses for a Pz26 based AEF arrangement as a function of frequency, again for the various components of the LTSpice model shown in Figure 2. Comparison of Figure 15 with the modelled losses of a similar AEF arrangement using

Pz27 (Figure 12) indicates that there is a significant difference in the amount of power lost in the PZT elements. For clarity, the modelled total-power-loss in the PZT elements (i.e. the sum of *PZTtrans* and *PZTrec* in Figure 12 and 15) has been re-plotted in Figure 16 which indicates that the viscous power loss in the PZT elements can be near 50% at certain drive frequencies. It is believed that this difference in viscous power loss in the PZT elements results in the improved power transfer efficiency for the Pz26 based AEF arrangement.

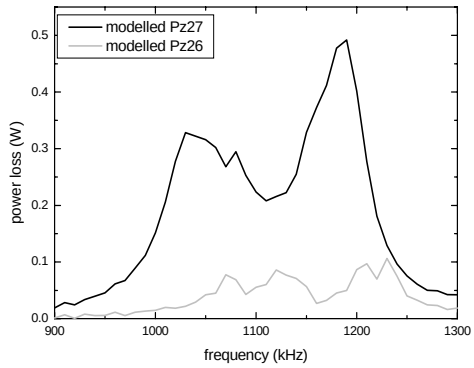

Figure 16. Comparison of modelled total power loss in the transmit and receive PZT elements of an AEF as a function of frequency and piezoelectric material type. Apparent input power was 1 W and the load resistance was 75 Ω and 30 Ω for Pz26 and Pz27 respectively

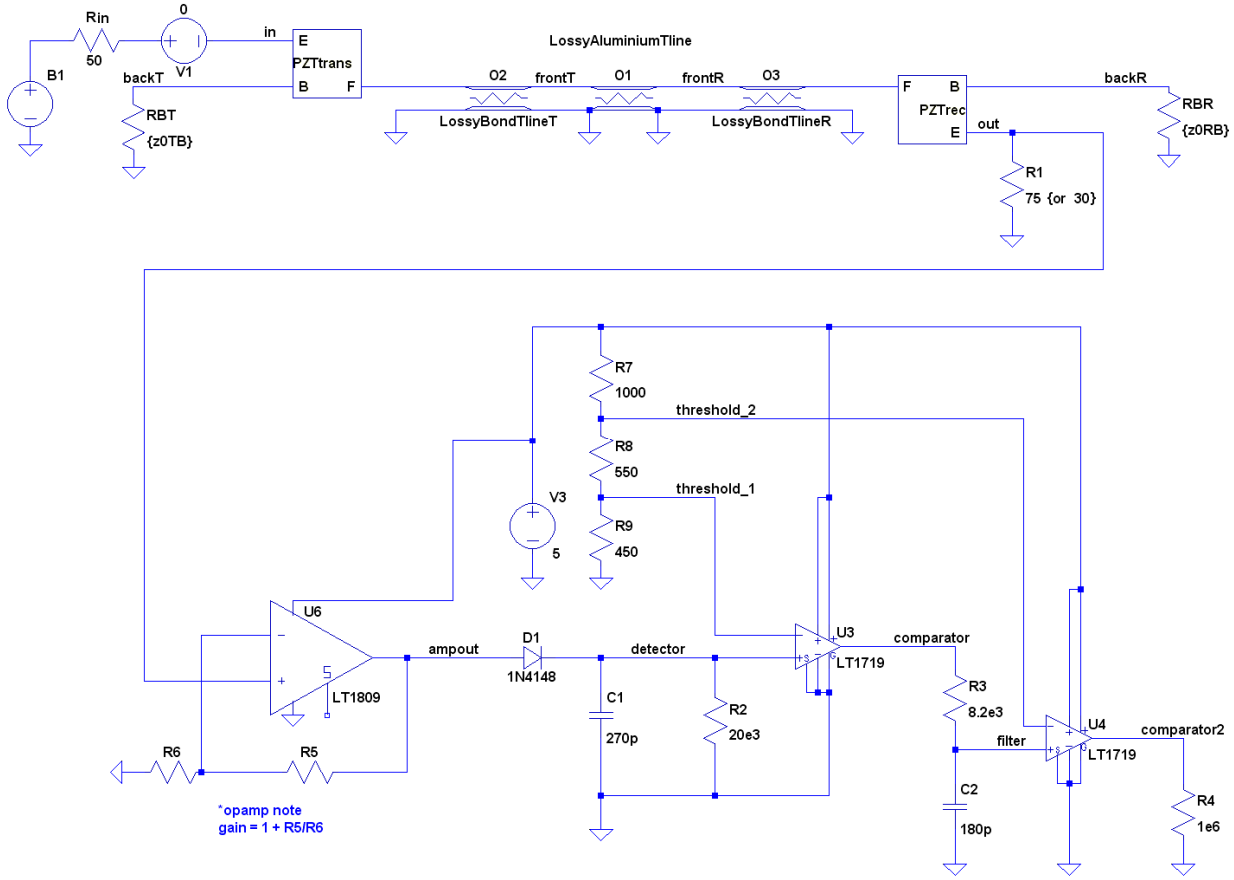

Figure 17. LTSpice schematic of the AEF communications test circuit. Load resistance R1 was 75 Ω for the Pz26 based AEF arrangement, and 30 Ω for the Pz27 arrangement.

3.3 Communications

3.3.1 Basic technique

Communications modelling and experimentation was carried out on AEF systems formed using both Pz26 and Pz27 material. Figure 17 shows a schematic of the arrangement used to simulate and experimentally characterize the communications method to be implemented in the AEF demonstrator. In summary, the method involves representing each high bit by a 10 V, ¼ cycle transmit pulse. As discussed earlier AEF arrangements formed using 2 mm thick PZT elements have an anti-resonant frequency of ~1100 kHz, so each transmit pulse has a duration of 260 ns. The pulse is applied to the transmit PZT element, which produces an acoustic stress wave which travels across the physical interface to the receive element where it is then detected. Since the mechanical Q's of both Pz26 and Pz27 are large (and damping low) then an acoustic stress

wave will continue to ring back and forth across the *physical interface* (Figure 1). To dampen the mechanical ringing an optimized electrical load is added to the receive element, shown in Figure 17 as *R1=75 Ω or 30 Ω*, for Pz26 or Pz27 respectively.

Figure 18 shows both the measured and the modelled pulse response of an AEF arrangement formed using 2 mm thick PZT disk elements. A 10 V, 260 ns, transmit pulse was used in both experiment and simulation. All of the results shown in Figure 18 have the same general form; the 260 ns transmit pulse produces a decaying waveform across the receive PZT element. Experimentally the sharp rise and fall of the 10 V, 260 ns transmit pulse produced two small *radio frequency* (RF) transients (narrow spikes indicated in Figure 18a) in the circuitry on the receiver side of the *physical interface*. These RF transients do not have a significant effect on the acoustic behaviour of the AEF system and were not modelled, however they do provide a useful indicator of timing of the transmit pulse relative to the received waveform. Figure 18a shows that the time between the rising edge of the transmit pulse and the initial response from the receive PZT element was at ~540 ns. Figure 18a also shows that for both the Pz26 and the Pz27 AEF arrangements, the received waveform had substantially decayed within 10 µs. Note that the maximum peak height of the received waveform for a Pz26 AEF arrangement is nearly twice the maximum peak height of the Pz27 arrangement; the larger received signal strength for the Pz26 AEF arrangement suggests that Pz26 is a more practical material for AEF communications. Figure 18b compares the modelled and measured receiver waveforms for a Pz26 AEF arrangement, and shows good correlation between the two. The modelled receiver signal strength is larger than the measured which indicates that the damping in the experimental arrangement is larger than that used in the model, agreeing with the power transfer results presented earlier (e.g. Figure 14b).

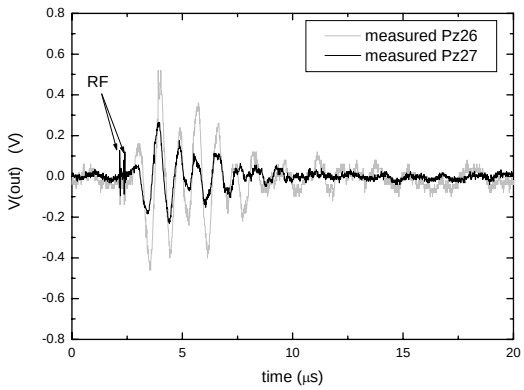

(a)

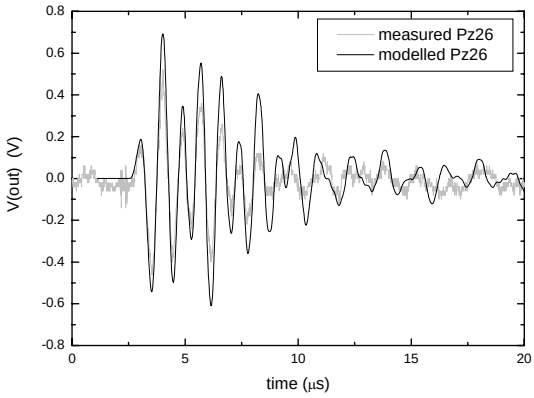

(b)

Figure 18. (a) Comparison of measured results from Pz26 and Pz27 based AEF arrangements using the communications test circuit shown in Figure 17, showing the received waveform produced with a 10V, 260 ns, transmit pulse. The two peaks marked 'RF' indicate the rising and falling edges of the transmit pulse. (b) Comparison of received waveforms, measured versus modelled, for a Pz26 based AEF arrangement. Node location V(out) is shown in Figure 17.

Figure 19 is a measured oscilloscope trace for a Pz26 AEF arrangement showing a series of transmit pulses (CH1), the output voltage generated across the receive PZT element (CH2) and the voltage response of the detector circuit shown in Figure 17 (CH4). The trace shown in Figure 19 was measured using a gain of 7 for operational amplifier U6 and a 5 V rail. The input voltage (CH1) shows that the height of the drive pulse across the transmit PZT element is somewhat less than the original 10 V due to the RC filtering effect of the 50 Ω output impedance (*Rin* in Figure 17) of the signal generator coupled with the capacitance of the transmit PZT element. Based on the measured detector signal (CH4), Figure 19 clearly shows that an AEF communications data rate of (at least) 115 kBits per second is achievable.

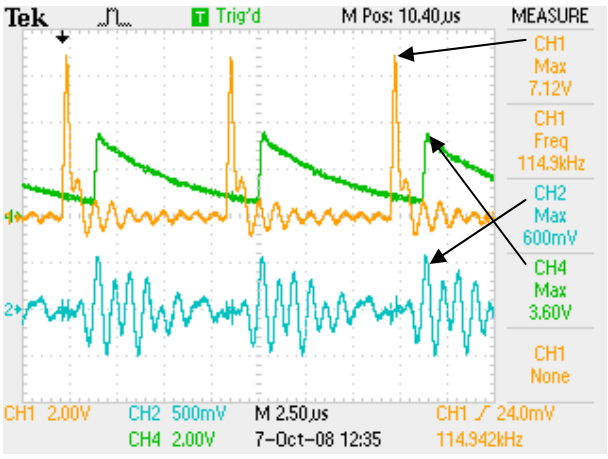

Figure 19. Measured results from the communications test circuit using a 10V, 260 ns, pulse across a Pz26 based AEF arrangement. CH1=V(in), CH2= V(out) and CH4=V(detector) as shown in Figure 17.

The circuit shown in Figure 17 was tested for robustness using simulation. Comparison was made between the output bit pattern at V(comparator2) with various V(in) input bit patterns which had a length of 10-bits and, at

least in simulation, the data transfer was robust. Of course the actual communication error rate will need to be tested in practice. The current CMPLE device outputs 20 kByte data blocks (10 bits per byte) with a check-sum test at the end of every block; so the error rate of the AEF system must be much less than *1 in 200 kBits*. It is envisaged that other, more robust, communication protocols will be implemented in future AEF systems. For example, a more robust approach might include the combination of a blocked, balanced and check-summed data stream with background averaging for the comparators inputs (as shown in Figure 17) to reduce the data transfer errors caused by slowly varying voltage offsets (e.g. due to temperature).

3.3.2 Future work

Based on the preliminary work described above, an electronics board for testing AEF communications and battery charging has been designed using existing CMPLE communications boards which include USB/RS232 interface converter chips. Future AEF communications circuit designs will incorporate these converter chips with a microcontroller on either side of the AEF *physical interface* to control communications. The board has been manufactured and is currently being tested. Both upstream and downstream AEF communications are being tested as well as the battery charging capability of the Pz26 based AEF arrangement.

Initial communications testing involves passing data between two computers across an AEF link. Future testing will be between an 'AEF interrogator' and a CMPLE unit. A fully operational AEF system will incorporate µ-power microprocessors to automatically select the operating state of the AEF link which will be dependant on the current situation (i.e. to determine whether the system is currently communicating upstream, downstream or providing power). However automation of the AEF system is beyond the scope of this paper and will be examined elsewhere.

CONCLUSION

This paper has examined the modelling, characterization and design of the *Acoustic Electric Feedthrough (AEF) Laboratory Demonstrator Mk II* with the ultimate aim of developing a system capable of passing power and communications through the aluminium skin of an aircraft using ultrasound. The AEF system is being designed to couple with, and increase the capability of, the DSTO CMPLE device which has been developed for measuring in-situ aircraft structural load. An AEF arrangement operates via two axially aligned piezoelectric elements, mounted on opposite sides of a metal plate. One piezoelectric element is excited at its thickness mode anti-resonance frequency which produces ultrasound that passes through the metal plate and is received by the second element located on the opposite side of the plate. The AEF demonstrator was considered to have three main sub-components: (i) a *transmitter*, (ii) a *physical interface* and (iii) a *receiver*. An LTSpice model of the AEF was developed and used to characterize the behaviour of the three main sub-components and predictions from the LTSpice model were confirmed by experiment. A comparison was made between two AEF systems, one formed using the piezoelectric material Pz26, the other with Pz27. Due to the superior power and signal transfer performance of Pz26, a decision was made to utilize Pz26 in the design of the *AEF Demonstrator Mk II*. Real power transfer efficiency was shown to be ~40% for the AEF demonstrator based on piezoelectric material Pz26. AEF power loss mechanisms were explored, with modelling indicating that up to 50% of the input power can be lost as heat in the piezoelectric elements caused by mechanical viscous loss. To confirm the modelled heat loss, thermal measurements were made of the temperature rise caused by heat generation in the piezoelectric elements. After 80 minutes of continuous operation using 3 W of real input power the measured temperature increase on the receive piezoelectric element was 4.6 K, indicating that the modelling was correct and that electrical power was being converted to heat in the PZT elements. However the relatively small temperature rise recorded suggests that the heat generated by an AEF system is not a significant issue. An AEF communications technique was modelled and then laboratory tested, indicating data transfer rates of greater than 115 kBits per second would be achieved. Finally an AEF board for testing communications and power transfer has been designed and manufactured and is currently being tested.

Appendix

definition	designation	units	material			
			Pz26[14]	Pz27[14]	aluminium[5]	silver epoxy[5]
clamped relative permittivity	$\varepsilon^{S}_{33,rel}$	-	699.7	914	-	-
piezoelectric constant	e_{33}	C/m^2	14.7	16	-	-
clamped elastic modulus	c^{D}_{33}	GPa	158	144	73.1	7.28
density	ρ	kg/m^3	7700	7700	2770	3890
mechanical quality	Q	-	3023	81.5	1000	23.4

References

1. S. C. Galea, S. van der Velden, S. Moss, I. Powlesland, 2008, to be published in the Encyclopaedia of Structural Health Monitoring.
2. S. D. Moss, S. C. Galea, I. G. Powlesland, M. Konak, A. A. Baker, SPIE's 2000 Symposium on Smart Materials and MEMS, Smart Structures and Devices Conference, Melbourne, Australia, SPIE 4325, 2000; Paper 4235-41.
3. S. C. Galea, S. D. Moss, I. G. Powlesland, A. A. Baker, 2002, Proc ACUN – 4 Composite Systems – Macrocomposites, UNSW, SYDNEY, Australia.
4. C. Davis, W. Baker, S. Moss, S. Galea, R. Jones, 2002, Proceedings of SPIE -- Volume 4934, Smart Materials II, Alan R. Wilson, Editor, November pp. 140-149.
5. N. Rajic, Journal of Intelligent Material Systems and Structures, 2000, Vol. 11(9) 696-702.
6. S. C. Galea, J. Agius, C. Davis and I. Powlesland, Proceedings of the 11th Joint NASA/FAA/DOD Conference on Aging Aircraft, Phoenix, Arizona, 21 – 24 April 2008.
7. S. D. Moss, P. McMahon, M. Konak, C. Phoumsavanh, N. Rajic, S. C. Galea, I. Powlesland, 2008, DSTO Research Report (in press).
8. S. D. Moss, , M. Konak, C. Phoumsavanh, N. Rajic, S. C. Galea, I. Powlesland, 2008, DSTO Technical Report (in press).
9. Y. Hu, X. Zhang, J. Yang, Q. Jiang, *IEEE Trans. Ultrason., Ferroelect., Freq. Cont.*, 2003, vol. 50 (7), pp. 773-781.
10. S. Sherrit, M. Badescu, X. Bao, Y. Bar-Cohen, Z. Chang, 2005, *Proceedings of SPIE Smart Structures Conference, San Diego, CA., Mar 6-10,* SPIE vol. 5758.
11. M. Engelhardt, LTspice/SwitcherCAD III, 2008, Linear Technology Corporation, www.linear.com
12. Püttmer, P. Hauptmann, R. Lucklum, O. Krause, B. Henning, *IEEE Trans. Ultrason., Ferroelect., Freq. Cont.*, 1997, vol. 44 (1), pp. 60-66.
13. J. van Deventer, T Löfqvist, *IEEE Trans. Ultrason., Ferroelect., Freq. Cont.*, 2000, vol. 47 (4), pp. 1014-1024.
14. Piezoelectric material parameters, Ferroperm website, 2006, www.ferroperm.com
15. Circuitworks Conductive Epoxy, CW2400.
16. N. Rajic, *Smart Mater. Struct.*, 2006, vol. 15, pp. 1151-1164.
17. http://www.fairchildsemi.com/pf/1N/1N5818.html, 2008.
18. www.onsemi.com/pub_link/Collateral/**MC34151**-D.PDF, 2008.
19. www.linear.com/pc/productDetail.jsp?navId=**LTC6902**, 2008.
20. www.national.com/pf/LP/**LP2950**.html, 2008.
21. N. Rajic, 2002, DSTO-TR-1298.
22. K. Krishnamurthy, F. Lalande, and C. A. Rogers, 1996, *Proc. SPIE*, vol. 2717, pp. 302-310.
23. N. Rajic, S. C. Galea and W. K. Chiu, *Smart Mater. Struct.*, 2002, vol. 11, pp. 107-114.